mathematics

MDPI

Article

Nanofluid Flow on a Shrinking Cylinder with Al_2O_3 Nanoparticles

Iskandar Waini [1,2], Anuar Ishak [2,*] and Ioan Pop [3]

[1] Fakulti Teknologi Kejuruteraan Mekanikal dan Pembuatan, Universiti Teknikal Malaysia Melaka, Melaka 76100, Malaysia; iskandarwaini@utem.edu.my
[2] Department of Mathematical Sciences, Faculty of Science and Technology, Universiti Kebangsaan Malaysia UKM, Bangi 43600, Malaysia
[3] Department of Mathematics, Faculty of Mathematics and Computer Science, Babeş-Bolyai University, 400084 Cluj-Napoca, Romania; ipop@math.ubbcluj.ro
* Correspondence: anuar_mi@ukm.edu.my

Abstract: This study investigates the nanofluid flow towards a shrinking cylinder consisting of Al_2O_3 nanoparticles. Here, the flow is subjected to prescribed surface heat flux. The similarity variables are employed to gain the similarity equations. These equations are solved via the bvp4c solver. From the findings, a unique solution is found for the shrinking strength $\lambda \geq -1$. Meanwhile, the dual solutions are observed when $\lambda_c < \lambda < -1$. Furthermore, the friction factor $Re_x^{1/2} C_f$ and the heat transfer rate $Re_x^{-1/2} Nu_x$ increase with the rise of Al_2O_3 nanoparticles φ and the curvature parameter γ. Quantitatively, the rates of heat transfer $Re_x^{-1/2} Nu_x$ increase up to 3.87% when φ increases from 0 to 0.04, and 6.69% when γ increases from 0.05 to 0.2. Besides, the profiles of the temperature $\theta(\eta)$ and the velocity $f'(\eta)$ on the first solution incline for larger γ, but their second solutions decline. Moreover, it is noticed that the streamlines are separated into two regions. Finally, it is found that the first solution is stable over time.

Keywords: heat transfer; prescribed heat flux; similarity solutions; dual solutions; stability analysis

Citation: Waini, I.; Ishak, A.; Pop, I. Nanofluid Flow on a Shrinking Cylinder with Al_2O_3 Nanoparticles. *Mathematics* **2021**, *9*, 1612. https://doi.org/10.3390/math9141612

Academic Editor: Aihua Wood

Received: 4 May 2021
Accepted: 6 July 2021
Published: 8 July 2021

1. Introduction

The fluid flow toward a stagnation point on a fixed surface was first introduced by Hiemenz [1] in 1911. The axisymmetric flow was then studied by Homann [2]. Ariel [3] followed by examining the flow with the hydromagnetic effects. The flow on a shrinking sheet was reported by Wang [4] and Kamal et al. [5]. Different from the aforementioned studies, which considered the flow over a flat plate, Wang [6] discussed the fluid flow over a circular cylinder. This was then followed by several researchers, including Ishak et al. [7] and Awaludin et al. [8], who studied the flow over a shrinking cylinder subject to a prescribed surface heat flux. They found that the increment of the curvature parameter delayed the boundary layer separation from the surface of the cylinder. Muthtamilselvan and Prakash [9] studied the unsteady flow and heat transfer of a nanofluid over a moving surface with prescribed heat and mass fluxes, and stated that the heat flux condition is important in a microelectromechanical (MEM) condensation application. Several researchers [10–16] have also considered this type of surface heating condition in their studies.

Nanoparticles and structures have been used by humans in fourth century AD, by the Romans, which demonstrated one of the most interesting examples of nanotechnology in the ancient world [17]. The term nanofluid, a mixture of the base fluid and nanoparticles, was initiated by Choi and Eastman [18]. It seems that Pak and Cho [19] were the first who introduced the thermophysical correlations for the nanofluid. Several studies have considered these nanofluid correlations [20–25]. The nanofluid correlations introduced by Pak and Cho [19] were improved by Ho et al. [26]. They reported that the numerical

predictions from the existing nanofluid correlations are contradicted with the experimental results. The dispersion of nanoparticles in the base fluid was observed to result in a marked reduction, instead of an enhancement. Therefore, they have introduced the new correlations of the Al_2O_3-water nanofluid through a least-square curve fitting from the experimental results. They concluded that these new correlations give more accurate predictions with the experimental data. It should be noted that the studies of the nanofluid employing these nanofluid correlations are very limited. Among them, Sheremet et al. [27] employed these correlations to study the natural convective heat transfer and fluid flow of Al_2O_3-water nanofluid in an inclined wavy-walled cavity under the effect of non-uniform heating. They found that the heat transfer rate and fluid flow rate are non-monotonic functions of the cavity inclination angle and undulation number. Similarly, these correlations have been considered by Waini et al. [28] to examine the impact of Dufour and Soret diffusions on Al_2O_3-water nanofluid flow over a moving thin needle. They reported that the skin friction coefficient and the heat transfer coefficients increase, but the mass transfer coefficient decreases in the presence of Al_2O_3 nanoparticles. This concept has been upgraded by considering two or more types of nanoparticles that dispersed simultaneously into the base fluid and is called 'hybrid nanofluid'. Some works on such fluids can be found in references [29–31]. Additionally, Takabi and Salehi [32] and Devi and Devi [33] introduced the hybrid nanofluid thermophysical models, which were widely used by many researchers [34–43] in the boundary layer problems. Furthermore, Waini et al. [44–47] scrutinized the temporal stability of the hybrid nanofluid flow.

In this study, the stagnation point flow towards a shrinking cylinder with the Al_2O_3 nanoparticle subjected to prescribed surface heat flux is investigated. Different from the previous studies, the present study examines the flow and thermal behavior of the Al_2O_3/water nanofluid by employing the correlations introduced by Ho et al. [26]. Most importantly, this is the first attempt to study the flow towards a stagnation region of a shrinking cylinder by considering these correlations. Moreover, the dual solutions and their stability are also reported in this study. The finding from this study can contribute to foresee the flow and thermal behaviors in industrial applications.

2. Mathematical Formulation

Consider the nanofluid flow on a shrinking cylinder with Al_2O_3 nanoparticles as shown in Figure 1.

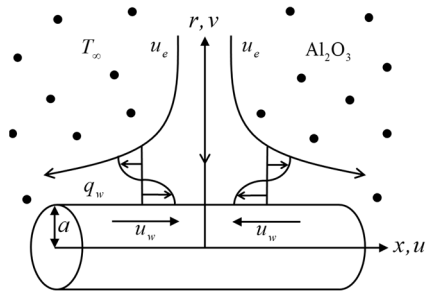

Figure 1. The flow configuration.

Here, $u_e(x) = c_1 x/L$ denotes the external flow velocity with $c_1 > 0$. The surface velocity is represented by $u_w(x) = c_2 x/L$ where c_2 is a constant. Besides, $q_w(x) = T_0 x/L$ is the prescribed heat flux where T_0 and T_∞ correspond to the reference and the ambient temperatures, respectively.

Accordingly, the governing equations are [7,8]:

$$\frac{\partial(ru)}{\partial x} + \frac{\partial(rv)}{\partial r} = 0 \tag{1}$$

$$u\frac{\partial u}{\partial x}+v\frac{\partial u}{\partial r}=u_e\frac{du_e}{dx}+\frac{\mu_{nf}}{\rho_{nf}}\left(\frac{\partial^2 u}{\partial r^2}+\frac{1}{r}\frac{\partial u}{\partial r}\right) \tag{2}$$

$$u\frac{\partial T}{\partial x}+v\frac{\partial T}{\partial r}=\frac{k_{nf}}{(\rho C_p)_{nf}}\left(\frac{\partial^2 T}{\partial r^2}+\frac{1}{r}\frac{\partial T}{\partial r}\right) \tag{3}$$

Subject to:

$$\begin{array}{l} u=u_w(x), v=0, k_{nf}\frac{\partial T}{\partial r}=-q_w(x) \text{ at } r=a \\ u\to u_e(x), T\to T_\infty \text{ as } r\to\infty \end{array} \tag{4}$$

where (u, v) are the corresponding velocity components and T is the temperature. Further, Table 1 provides the properties of water and Al_2O_3 [22]. Here, Prandtl number, Pr is taken as Pr = 6.2. Meanwhile, the nanofluid thermophysical models are given by [19,26]:

$$\begin{array}{l} \mu_{nf}=\mu_f\left(1+4.93\varphi+222.4\varphi^2\right),\ \ k_{nf}=k_f\left(1+2.944\varphi+19.672\varphi^2\right), \\ \rho_{nf}=(1-\varphi)\rho_f+\varphi\rho_s,\ \ (\rho C_p)_{nf}=(1-\varphi)(\rho C_p)_f+\varphi(\rho C_p)_s \end{array} \tag{5}$$

where μ, k, ρ, and (ρC_p) denote the dynamic viscosity, the thermal conductivity, the density, and the heat capacity, respectively with φ is the Al_2O_3 nanoparticle volume fractions and the subscript s represents its solid component. Meanwhile, the subscripts f and nf correspond to fluid and nanofluid, respectively. Note that these thermophysical models were also considered by Sheremet et al. [27] and Waini et al. [28].

Table 1. Thermophysical properties.

Properties	Nanoparticle	Base Fluid
	Al_2O_3	water
C_p (J/kgK)	765	4179
ρ (kg/m^3)	3970	997.1
k (W/mK)	40	0.613

Consider the following dimensionless variables [7,8]:

$$\psi=\left(\frac{c_1\nu_f}{L}\right)^{1/2}axf(\eta), T=T_\infty+\frac{q_w}{k_f}\left(\frac{\nu_f L}{c_1}\right)^{1/2}\theta(\eta),\ \eta=\left(\frac{c_1}{\nu_f L}\right)^{1/2}\frac{r^2-a^2}{2a} \tag{6}$$

With the stream function ψ, the characteristic length L, and the fluid kinematic viscosity ν_f. Here, $u=(\partial\psi/\partial r)/r$ and $v=-(\partial\psi/\partial x)/r$. So that:

$$u=\frac{c_1 x}{L}f\prime(\eta), v=-\frac{a}{r}\left(\frac{c_1\nu_f}{L}\right)^{1/2}f(\eta) \tag{7}$$

On using Equations (6) and (7), the continuity equation, i.e., Equation (1), is identically satisfied. Now, Equations (2) and (3) become:

$$\frac{\mu_{nf}/\mu_f}{\rho_{nf}/\rho_f}[2\gamma f''+(1+2\gamma\eta)f''']+1-f\prime^2+ff''=0 \tag{8}$$

$$\frac{1}{\Pr}\frac{k_{nf}/k_f}{(\rho C_p)_{nf}/(\rho C_p)_f}\left[2\gamma\theta'+(1+2\gamma\eta)\theta''\right]+f\theta'-f'\theta=0 \tag{9}$$

Subject to:

$$\begin{array}{l} f'(0)=\lambda, f(0)=0, \theta'(0)=-\frac{k_f}{k_{nf}}, \\ f'(\eta)\to 1, \theta(\eta)\to 0 \ \text{ as } \ \eta\to\infty \end{array} \tag{10}$$

The physical parameters appearing in Equations (8)–(10) are the stretching/shrinking parameter λ, the curvature parameter γ, and the Prandtl number Pr, given as:

$$\lambda = \frac{c_2}{c_1}, \quad \gamma = \left(\frac{\nu_f L}{c_1 a^2}\right)^{1/2}, \quad \Pr = \frac{(\mu C_p)_f}{k_f} \tag{11}$$

Note that, $\lambda < 0$ and $\lambda > 0$ signify the shrinking and stretching sheets, while $\lambda = 0$ is for the static sheet. Here, by taking $\varphi = \lambda = \gamma = 0$, Equation (8) reduces to the Hiemenz flow, see White [48]. The local Nusselt number Nu_x and the skin friction coefficients C_f are:

$$Nu_x = -\frac{xk_{nf}}{k_f(T_w - T_\infty)}\left(\frac{\partial T}{\partial r}\right)_{r=a}, \quad C_f = \frac{\mu_{nf}}{\rho_f u_e^2}\left(\frac{\partial u}{\partial r}\right)_{r=a} \tag{12}$$

On using Equation (6), one obtains

$$Re_x^{-1/2} Nu_x = \frac{1}{\theta(0)}, \quad Re_x^{1/2} C_f = \frac{\mu_{nf}}{\mu_f} f''(0) \tag{13}$$

where $Re_x = u_e x/\nu_f$ is the local Reynolds number.

3. Stability Analysis

This temporal stability analysis was first introduced by Merkin [49] and then followed by Weidman et al. [50]. Firstly, consider the new variables as follows [8]:

$$\psi = \left(\frac{c_1\nu_f}{L}\right)^{1/2} axf(\eta,\tau), T = T_\infty + \frac{q_w}{k_f}\left(\frac{\nu_f L}{c_1}\right)^{1/2}\theta(\eta,\tau), \ \eta = \left(\frac{c_1}{\nu_f L}\right)^{1/2}\frac{r^2 - a^2}{2a}, \ \tau = \frac{c_1}{L}t \tag{14}$$

where τ is the dimensionless time variable. Then, the unsteady form of Equations (2) and (3) are employed. On using Equation (14), one obtains:

$$\frac{\mu_{nf}/\mu_f}{\rho_{nf}/\rho_f}\left[2\gamma\frac{\partial^2 f}{\partial\eta^2} + (1+2\gamma\eta)\frac{\partial^3 f}{\partial\eta^3}\right] + 1 - \left(\frac{\partial f}{\partial\eta}\right)^2 + f\frac{\partial^2 f}{\partial\eta^2} - \frac{\partial^2 f}{\partial\eta\partial\tau} = 0 \tag{15}$$

$$\frac{1}{\Pr}\frac{k_{nf}/k_f}{(\rho C_p)_{nf}/(\rho C_p)_f}\left[2\gamma\frac{\partial\theta}{\partial\eta} + (1+2\gamma\eta)\frac{\partial^2\theta}{\partial\eta^2}\right] + f\frac{\partial\theta}{\partial\eta} - \theta\frac{\partial f}{\partial\eta} - \frac{\partial\theta}{\partial\tau} = 0 \tag{16}$$

Subject to:

$$\begin{array}{l} \frac{\partial f}{\partial\eta}(0,\tau) = \lambda, \quad f(0,\tau) = 0, \ \frac{\partial\theta}{\partial\eta}(0,\tau) = -\frac{k_f}{k_{nf}}, \\ \frac{\partial f}{\partial\eta}(\infty,\tau) = 1, \quad \theta(\infty,\tau) = 0 \end{array} \tag{17}$$

To investigate the temporal stability, the following perturbation functions are employed [50]:

$$f(\eta,\tau) = f_0(\eta) + e^{-\alpha\tau}F(\eta), \quad \theta(\eta,\tau) = \theta_0(\eta) + e^{-\alpha\tau}G(\eta) \tag{18}$$

where $F(\eta)$ and $G(\eta)$ are comparatively small compared to $f_0(\eta)$ and $\theta_0(\eta)$, and α denotes the eigenvalue. On using Equation (18), Equations (15) and (16) respectively become:

$$\frac{\mu_{nf}/\mu_f}{\rho_{nf}/\rho_f}[2\gamma F'' + (1+2\gamma\eta)F'''] - 2f_0'F' + f_0''F + f_0F'' + \alpha F' = 0 \tag{19}$$

$$\frac{1}{\Pr}\frac{k_{nf}/k_f}{(\rho C_p)_{nf}/(\rho C_p)_f}[2\gamma G' + (1+2\gamma\eta)G''] + f_0G' + \theta_0'F - f_0'G - \theta_0F' + \alpha G = 0 \tag{20}$$

The boundary conditions then become:

$$\begin{aligned} F'(0) = 0, \quad F(0) = 0, G'(0) = 0; \\ F'(\infty) = 0, \quad G(\infty) = 0 \end{aligned} \tag{21}$$

Without loss of generality, following Harris et al. [51], we fix the value of $F''(0)$ as $F''(0) = 1$ to obtain the smallest eigenvalues α in Equations (19) and (20).

4. Results and Discussion

The solutions of Equations (8)–(10) are attained by utilizing the package bvp4c in MATLAB software [52]. The effects of various physical parameters are then examined and presented in tabular and graphical forms.

By taking $\varphi = \lambda = \gamma = 0$, we obtain $f''(0) = 1.232588$, which is in agreement with what is reported by Wang [4] and Awaludin et al. [8]. The values of $f''(0)$ and $1/\theta(0)$ for several values of λ when $\varphi = \gamma = 0$ are also provided in Table 2 for future reference. Further, the values of $Re_x^{-1/2}Nu_x$ and $Re_x^{1/2}C_f$ when Pr $= 6.2$ with various values of φ, γ, and λ are given in Table 3. The values of $Re_x^{-1/2}Nu_x$ and $Re_x^{1/2}C_f$ are intensified with the rise of γ and φ. Quantitatively, a 3.87% increment of $Re_x^{-1/2}Nu_x$ is observed when φ increases from 0 to 0.04. Moreover, it is noticeable that the values of $Re_x^{-1/2}Nu_x$ increase up to 6.69% when γ increases from 0.05 to 0.2. Meanwhile, the values of $Re_x^{1/2}C_f$ reduce, but the values of $Re_x^{-1/2}Nu_x$ increase when λ increases from -0.5 to 0.5. It is seen that the nanoparticle volume fractions, the curvature, and the stretching/shrinking parameters can be utilized to control the heat transfer rate.

Table 2. Values of $f''(0)$ and $1/\theta(0)$ for regular fluid ($\varphi = 0$) under different λ when $\gamma = 0$ (flat plate).

λ	Wang [4]	Awaludin et al. [8]	Present Results	
	$f''(0)$	$f''(0)$	$f''(0)$	$1/\theta(0)$
-1	1.32882		1.328817	-2.359393
-0.5	1.49567		1.495670	0.314542
0	1.232588	1.232588	1.232588	1.573433
0.1	1.14656	1.146561	1.146561	1.767533
0.2	1.051130	1.051130	1.051130	1.949500
0.5	0.7133	0.713295	0.713295	2.438276
1	0	0	0	3.120727
2	-1.88731	-1.887307	-1.887307	4.203068
5	-10.26475	-10.264749	-10.264749	6.491300

Table 3. Values of $Re_x^{-1/2}Nu_x$ and $Re_x^{1/2}C_f$ for φ, γ, and λ when Pr $= 6.2$.

φ	γ	λ	$Re_x^{-1/2}Nu_x$	$Re_x^{1/2}C_f$
0	0	0	1.573433	1.232588
0.02			1.610281	1.382684
0.04			1.634333	1.625081
0.04	0.05		1.673416	1.667025
	0.1		1.711566	1.708036
	0.2		1.785416	1.787623
	0.1	-0.5	0.354240	2.110589
		-0.2	1.242946	1.914480
		0.5	2.645346	0.979397

Next, the results in graphical forms are provided to have a better insight into the effect of the physical parameters. The variations of the local Nusselt number $Re_x^{-1/2}Nu_x$ and the skin friction coefficient $Re_x^{1/2}C_f$ against λ when $\varphi = 0.02$ and Pr $= 6.2$ for several values of γ are shown in Figures 2 and 3. Larger γ gives higher values of $Re_x^{1/2}C_f$ and $Re_x^{-1/2}Nu_x$

on the first solution compared to the flat plate case ($\gamma = 0$). Besides, a unique solution is found when $\lambda \geq -1$. Meanwhile, two solutions are observed for the limited range of λ when the sheet is shrunk ($\lambda_c < \lambda < -1$). The similarity solutions also terminate in this region at $\lambda = \lambda_c$ (critical value). Here, the critical values are respectively $\lambda_c = -1.24657$, -1.32099, and -1.38801 for $\gamma = 0$, 0.1 and 0.2. The velocity $f'(\eta)$ and temperature $\theta(\eta)$ profiles for $\varphi = 0, 0.02$, and 0.04 when Pr $= 6.2$, $\lambda = -1.24$, and $\gamma = 0.1$ are given in Figures 4 and 5. The reduction of $f'(\eta)$ and $\theta(\eta)$ are observed for both branches with the rising of φ. Physically, the addition of the nanoparticles makes the fluid more viscous and thus, slows down the flow. Consequently, the fluid velocity decreases. Also, the added nanoparticles dissipate energy in the form of heat and consequently exert more energy, which enhances the temperature. However, in this study, we discover that the temperature decreases as φ increases. This behavior is due to the prescribed heat flux on the shrinking surface of the cylinder.

Further, Figures 6 and 7 show the effect of γ on $f'(\eta)$ and $\theta(\eta)$ when $\varphi = 0.02$, $\lambda = -1.24$ and Pr $= 6.2$. The profiles of $f'(\eta)$ and $\theta(\eta)$ on the first solution incline for larger γ. However, the profiles on the second solution decline. Besides, the negative values of $\theta(\eta)$ are noticed in Figures 5 and 7. The definition of the curvature parameter γ is inversely proportional to the radius of the cylinder, see Equation (11). Thus, the radius of the cylinder decreases as γ increases. Hence, the fluid velocity amplifies due to less resistance occurring between the surface of the cylinder and the fluid. Consequently, the fluid temperature increases for cumulative γ. Since the Kelvin temperature of substances is defined as the average kinetic energy of the particles of substances, as velocity enhances with γ, the kinetic energy increases, and consequently intensifies the temperature [16].

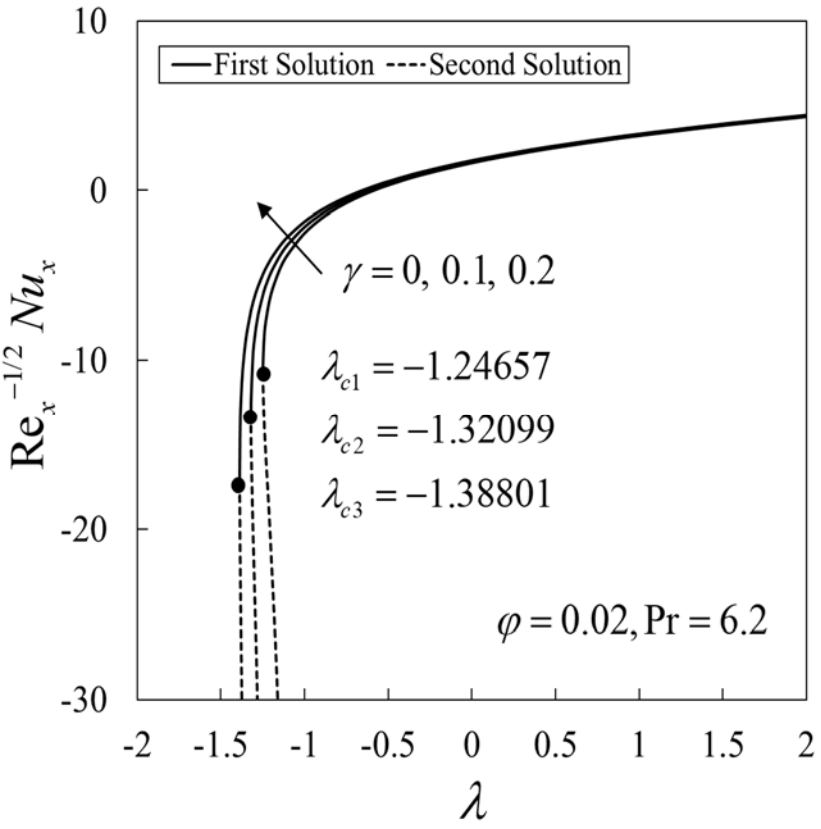

Figure 2. Local Nusselt number $Re_x^{-1/2} Nu_x$ against λ for various values of γ.

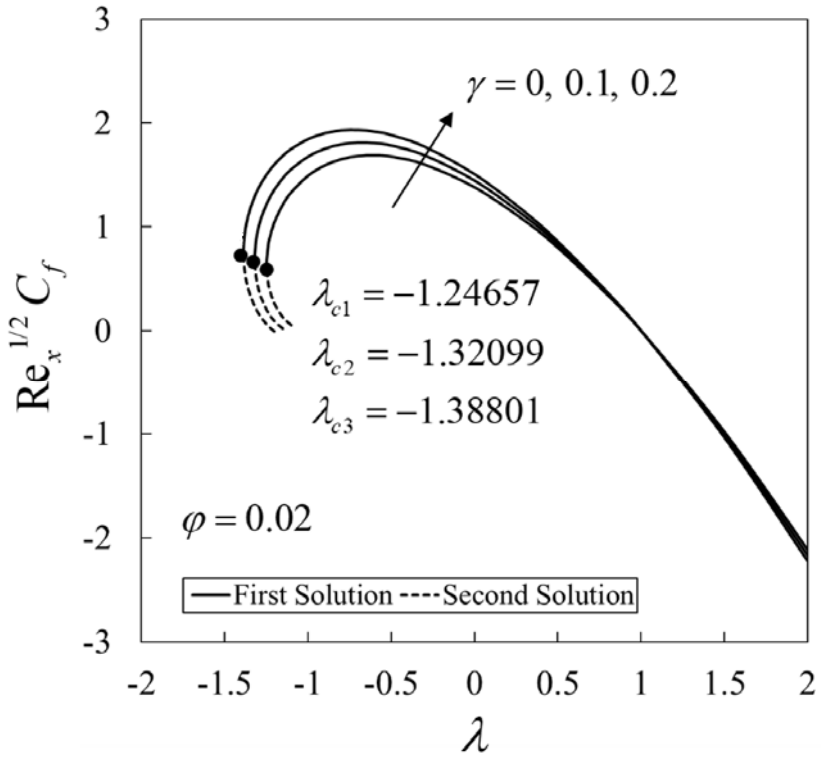

Figure 3. Skin friction coefficient $Re_x^{1/2} C_f$ against λ for various values of γ.

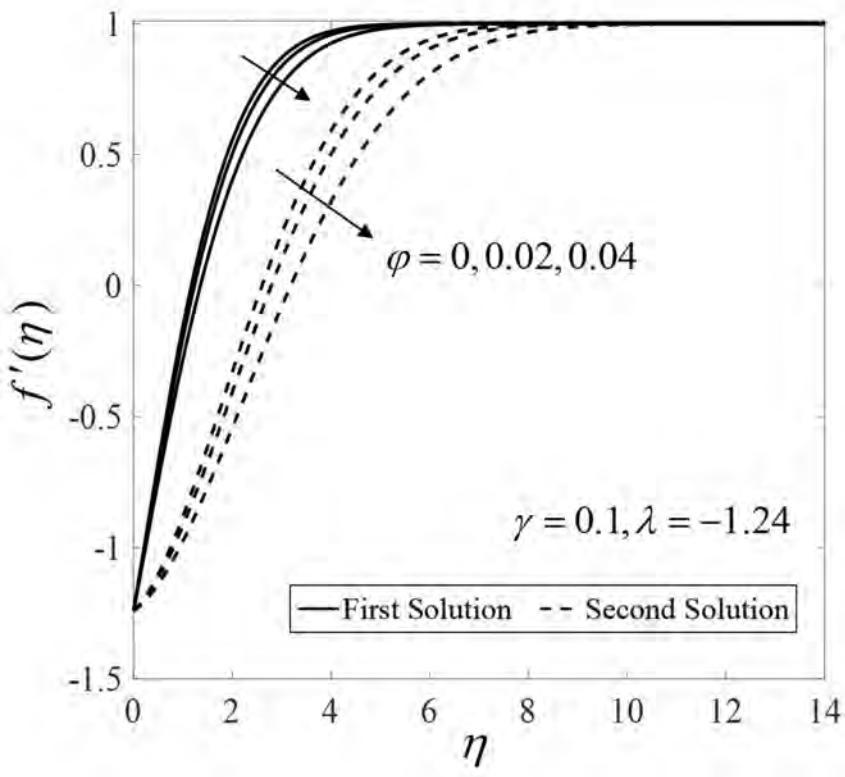

Figure 4. Velocity profiles $f'(\eta)$ for various values of φ.

Figures 8 and 9 display the streamlines when $\lambda = -1.24$ (shrinking sheet), $\varphi = 0.02$, and $\gamma = 0.1$ for the first and the second solutions, respectively. Here, the streamlines are plotted for several values of $\overline{\psi} = \psi / a(c_1 \nu_f / L)^{1/2}$. The streamlines are separated into two regions by the horizontal line for both solutions. It is notable that the horizontal line that

separates the flow is nearer to the shrinking sheet for the first solution. Besides, the reverse rotating flow occurs in the lower region. Meanwhile, the flow pattern on the upper region behaves as the normal stagnation point.

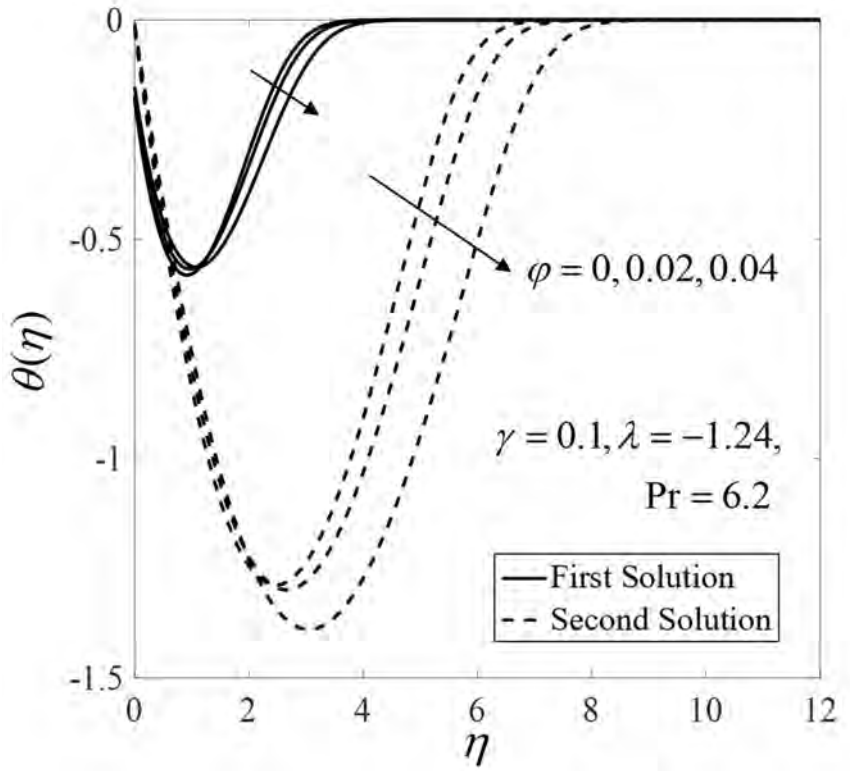

Figure 5. Temperature profiles $\theta(\eta)$ for various values of φ.

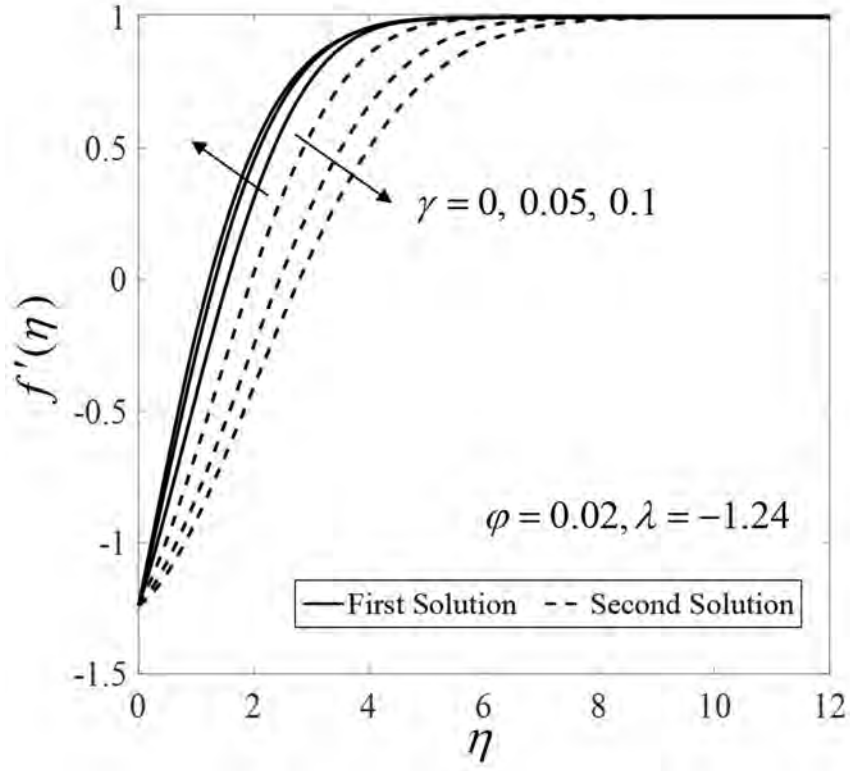

Figure 6. Velocity profiles $f'(\eta)$ for various values of γ.

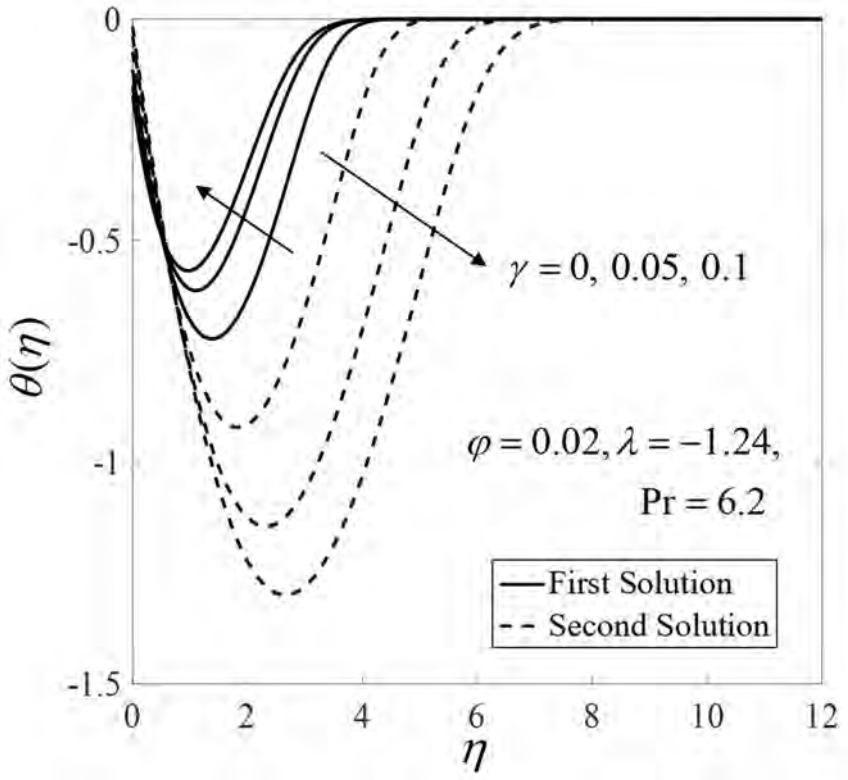

Figure 7. Temperature profiles $\theta(\eta)$ for various values of γ.

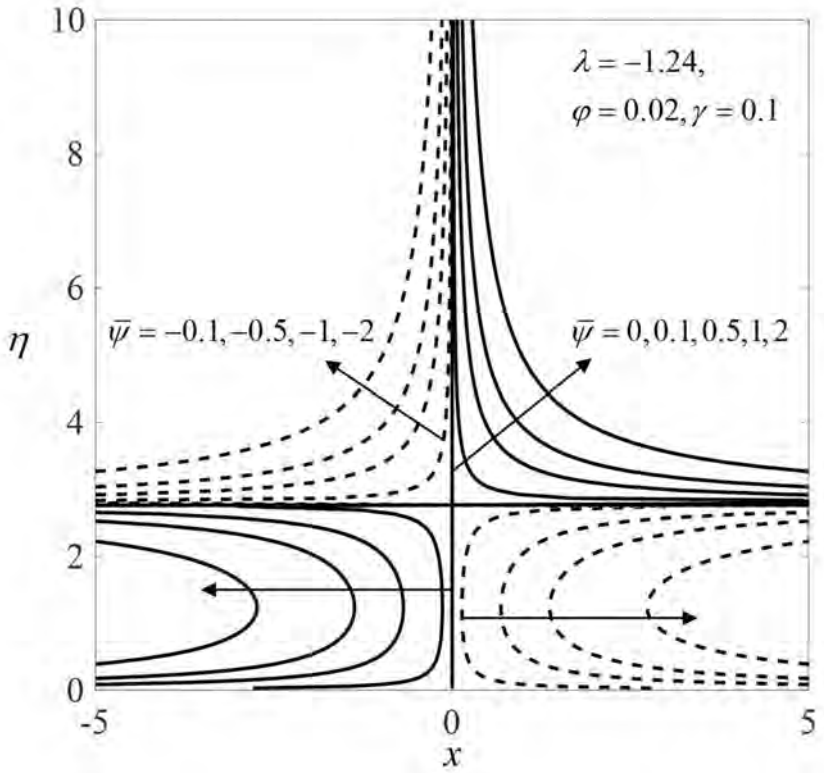

Figure 8. Streamlines for the first solution.

The variation of α against λ when $\varphi = 0.02$ and $\gamma = 0.1$ is described in Figure 10. For positive values of α, it is noted that $e^{-\alpha\tau} \to 0$ as time evolves $(\tau \to \infty)$. In contrast, negative values of α, $e^{-\alpha\tau} \to \infty$ as $\tau \to \infty$ show a growth of disturbance as time evolves.

These behaviors show that the first solution is stable, while the second solution is unstable in the long run.

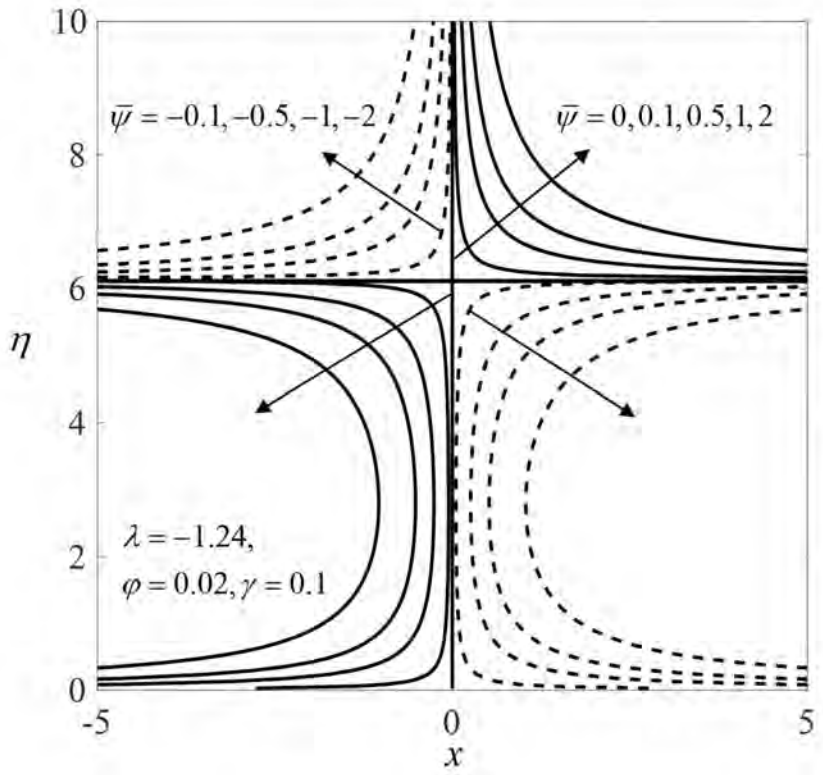

Figure 9. Streamlines for the second solution.

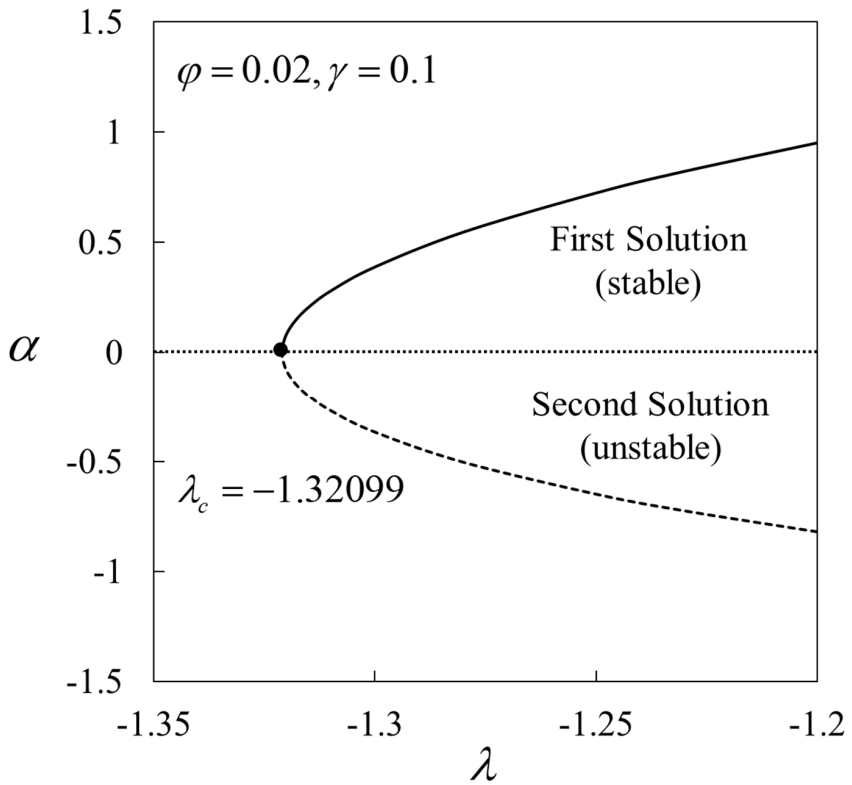

Figure 10. Smallest eigenvalues α against λ.

5. Conclusions

This study examined the stagnation point flow on a shrinking cylinder filled with Al_2O_3 nanoparticles. The surface of the cylinder is subjected to prescribed surface heat flux. The correlations of Al_2O_3/water nanofluid introduced by Ho et al. [25] were employed. Findings revealed two solutions to be observed for the limited range of λ when the sheet is shrunk ($\lambda_c < \lambda < -1$). The similarity solutions terminated in this region at $\lambda = \lambda_c$. Meanwhile, a unique solution was found when $\lambda \geq -1$. The skin friction coefficient $Re_x^{1/2} C_f$ and the local Nusselt number $Re_x^{-1/2} Nu_x$ were intensified with the rising of the nanoparticle volume fraction φ and the curvature parameter γ. Quantitatively, the values of $Re_x^{-1/2} Nu_x$ increased up to 3.87% when φ is increased from 0 to 0.04, and 6.69% when γ is increased from 0.05 to 0.2. Furthermore, Al_2O_3/water nanofluid produced higher values of $Re_x^{1/2} C_f$ and $Re_x^{-1/2} Nu_x$ compared to water. Moreover, the rising of φ tended to reduce the velocity $f'(\eta)$ and the temperature $\theta(\eta)$ for both branches. Besides, the profiles on the first solution incline when larger values of γ are applied. Finally, the temporal stability analysis showed that the first solution is stable while the second solution is unstable over time.

Author Contributions: Conceptualization, I.P.; funding acquisition, A.I.; methodology, I.W.; Project administration, A.I.; supervision, A.I. and I.P.; validation, I.P.; writing—original draft, I.W.; writing—review and editing, A.I., I.P. All authors have read and agreed to the published version of the manuscript.

Funding: This research was funded by Universiti Kebangsaan Malaysia (Project Code: DIP-2020-001).

Institutional Review Board Statement: Not applicable.

Informed Consent Statement: Not applicable.

Data Availability Statement: Not applicable.

Acknowledgments: We acknowledge the Universiti Teknikal Malaysia Melaka and the Universiti Kebangsaan Malaysia (DIP-2020-001) for financial supports.

Conflicts of Interest: The authors declare no conflict of interest.

References

1. Hiemenz, K. Die Grenzschicht an einem in den gleichförmigen Flüssigkeitsstrom eingetauchten geraden Kreiszylinder. *Dinglers Polytech. J.* **1911**, *326*, 321–410.
2. Homann, F. Der Einflub grober Zähigkeit bei der Strömung um den Zylinder und um die Kugel. *Z. Angew. Math. Mech.* **1936**, *16*, 153–164. [CrossRef]
3. Ariel, P.D. Hiemenz flow in hydromagnetics. *Acta Mech.* **1994**, *103*, 31–43. [CrossRef]
4. Wang, C.Y. Stagnation flow towards a shrinking sheet. *Int. J. Nonlinear Mech.* **2008**, *43*, 377–382. [CrossRef]
5. Kamal, F.; Zaimi, K.; Ishak, A.; Pop, I. Stability analysis of MHD stagnation-point flow towards a permeable stretching/shrinking sheet in a nanofluid with chemical reactions effect. *Sains Malays.* **2019**, *48*, 243–250. [CrossRef]
6. Wang, C.Y. Fluid flow due to a stretching cylinder. *Phys. Fluids* **1988**, *31*, 466. [CrossRef]
7. Ishak, A. Mixed convection boundary layer flow over a vertical cylinder with prescribed surface heat flux. *J. Phys. A Math. Theor.* **2009**, *42*, 195501. [CrossRef]
8. Awaludin, I.S.; Ahmad, R.; Ishak, A. On the stability of the flow over a shrinking cylinder with prescribed surface heat flux. *Propuls. Power Res.* **2020**, *9*, 181–187. [CrossRef]
9. Muthtamilselvan, M.; Prakash, D. Unsteady hydromagnetic slip flow and heat transfer of nanofluid over a moving surface with prescribed heat and mass fluxes. *Proc. Inst. Mech. Eng. Part C J. Mech. Eng. Sci.* **2015**, *229*, 703–715. [CrossRef]
10. Bachok, N.; Ishak, A. Flow and heat transfer over a stretching cylinder with prescribed surface heat flux. *Malays. J. Math. Sci.* **2010**, *4*, 159–169.
11. Bhattacharyya, K. Heat transfer in boundary layer stagnation-point flow towards a shrinking sheet with non-uniform heat flux. *Chin. Phys. B* **2013**, *22*, 074705. [CrossRef]
12. Qasim, M.; Khan, Z.H.; Khan, W.A.; Ali Shah, I. MHD boundary layer slip flow and heat transfer of ferrofluid along a stretching cylinder with prescribed heat flux. *PLoS ONE* **2014**, *9*, e83930.
13. Mabood, F.; Lorenzini, G.; Pochai, N.; Ibrahim, S.M. Effects of prescribed heat flux and transpiration on MHD axisymmetric flow impinging on stretching cylinder. *Contin. Mech. Thermodyn.* **2016**, *28*, 1925–1932. [CrossRef]
14. Megahed, A.M. Carreau fluid flow due to nonlinearly stretching sheet with thermal radiation, heat flux, and variable conductivity. *Appl. Math. Mech.* **2019**, *40*, 1615–1624. [CrossRef]

15. Waini, I.; Ishak, A.; Pop, I. On the stability of the flow and heat transfer over a moving thin needle with prescribed surface heat flux. *Chin. J. Phys.* **2019**, *60*, 651–658. [CrossRef]
16. Giri, S.S.; Das, K.; Kundu, P.K. Homogeneous–heterogeneous reaction mechanism on MHD carbon nanotube flow over a stretching cylinder with prescribed heat flux using differential transform method. *J. Comput. Des. Eng.* **2020**, *7*, 337–351.
17. Bayda, S.; Adeel, M.; Tuccinardi, T.; Cordani, M.; Rizzolio, F. The history of nanoscience and nanotechnology: From chemical–physical applications to nanomedicine. *Molecules* **2020**, *25*, 112. [CrossRef] [PubMed]
18. Choi, S.U.S.; Eastman, J.A. Enhancing thermal conductivity of fluids with nanoparticles. In Proceedings of the ASME International Mechanical Engineering Congress & Exposition, San Francisco, CA, USA, 12–17 November 1995; pp. 99–105.
19. Pak, B.C.; Cho, Y.I. Hydrodynamic and heat transfer study of dispersed fluids with submicron metallic oxide. *Exp. Heat Transf.* **1998**, *11*, 151–170. [CrossRef]
20. Khanafer, K.; Vafai, K.; Lightstone, M. Buoyancy-driven heat transfer enhancement in a two-dimensional enclosure utilizing nanofluids. *Int. J. Heat Mass Transf.* **2003**, *46*, 3639–3653. [CrossRef]
21. Tiwari, R.K.; Das, M.K. Heat transfer augmentation in a two-sided lid-driven differentially heated square cavity utilizing nanofluids. *Int. J. Heat Mass Transf.* **2007**, *50*, 2002–2018. [CrossRef]
22. Oztop, H.F.; Abu-Nada, E. Numerical study of natural convection in partially heated rectangular enclosures filled with nanofluids. *Int. J. Heat Fluid Flow* **2008**, *29*, 1326–1336. [CrossRef]
23. Mohebbi, R.; Rashidi, M.M. Numerical simulation of natural convection heat transfer of a nanofluid in an L-shaped enclosure with a heating obstacle. *J. Taiwan Inst. Chem. Eng.* **2017**, *72*, 70–84. [CrossRef]
24. Gavili, A.; Isfahani, T. Experimental investigation of transient heat transfer coefficient in natural convection with Al_2O_3-nanofluids. *Heat Mass Transf.* **2020**, *56*, 901–911. [CrossRef]
25. Turkyilmazoglu, M. Single phase nanofluids in fluid mechanics and their hydrodynamic linear stability analysis. *Comput. Methods Programs Biomed.* **2020**, *187*, 105171. [CrossRef] [PubMed]
26. Ho, C.J.; Liu, W.K.; Chang, Y.S.; Lin, C.C. Natural convection heat transfer of alumina-water nanofluid in vertical square enclosures: An experimental study. *Int. J. Therm. Sci.* **2010**, *49*, 1345–1353. [CrossRef]
27. Sheremet, M.A.; Trîmbiţaş, R.; Groşan, T.; Pop, I. Natural convection of an alumina-water nanofluid inside an inclined wavy-walled cavity with a non-uniform heating using Tiwari and Das' nanofluid model. *Appl. Math. Mech.* **2018**, *39*, 1425–1436. [CrossRef]
28. Waini, I.; Ishak, A.; Pop, I. Dufour and Soret effects on Al_2O_3-water nanofluid flow over a moving thin needle: Tiwari and Das model. *Int. J. Numer. Methods Heat Fluid Flow* **2021**, *31*, 766–782. [CrossRef]
29. Turcu, R.; Darabont, A.; Nan, A.; Aldea, N.; Macovei, D.; Bica, D.; Vekas, L.; Pana, O.; Soran, M.L.; Koos, A.A.; et al. New polypyrrole-multiwall carbon nanotubes hybrid materials. *J. Optoelectron. Adv. Mater.* **2006**, *8*, 643–647.
30. Jana, S.; Salehi-Khojin, A.; Zhong, W.H. Enhancement of fluid thermal conductivity by the addition of single and hybrid nano-additives. *Thermochim. Acta* **2007**, *462*, 45–55. [CrossRef]
31. Suresh, S.; Venkitaraj, K.P.; Selvakumar, P.; Chandrasekar, M. Synthesis of Al_2O_3-Cu/water hybrid nanofluids using two step method and its thermo physical properties. *Colloids Surf. A Physicochem. Eng. Asp.* **2011**, *388*, 41–48. [CrossRef]
32. Takabi, B.; Salehi, S. Augmentation of the heat transfer performance of a sinusoidal corrugated enclosure by employing hybrid nanofluid. *Adv. Mech. Eng.* **2014**, *6*, 147059. [CrossRef]
33. Devi, S.P.A.; Devi, S.S.U. Numerical investigation of hydromagnetic hybrid Cu-Al_2O_3/water nanofluid flow over a permeable stretching sheet with suction. *Int. J. Nonlinear Sci. Numer. Simul.* **2016**, *17*, 249–257. [CrossRef]
34. Jamshed, W.; Aziz, A. Cattaneo–Christov based study of TiO_2–CuO/EG Casson hybrid nanofluid flow over a stretching surface with entropy generation. *Appl. Nanosci.* **2018**, *8*, 685–698. [CrossRef]
35. Subhani, M.; Nadeem, S. Numerical analysis of micropolar hybrid nanofluid. *Appl. Nanosci.* **2019**, *9*, 447–459. [CrossRef]
36. Hassan, M.; Faisal, A.; Ali, I.; Bhatti, M.M.; Yousaf, M. Effects of Cu–Ag hybrid nanoparticles on the momentum and thermal boundary layer flow over the wedge. *Proc. Inst. Mech. Eng. Part E J. Process Mech. Eng.* **2019**, *233*, 1128–1136. [CrossRef]
37. Maskeen, M.M.; Zeeshan, A.; Mehmood, O.U.; Hassan, M. Heat transfer enhancement in hydromagnetic alumina–copper/water hybrid nanofluid flow over a stretching cylinder. *J. Therm. Anal. Calorim.* **2019**, *138*, 1127–1136. [CrossRef]
38. Khashi'ie, N.S.; Arifin, N.M.; Nazar, R.; Hafidzuddin, E.H.; Wahi, N.; Pop, I. Magnetohydrodynamics (MHD) axisymmetric flow and heat transfer of a hybrid nanofluid past a radially permeable stretching/shrinking sheet with Joule heating. *Chin. J. Phys.* **2020**, *64*, 251–263. [CrossRef]
39. Zainal, N.A.; Nazar, R.; Naganthran, K.; Pop, I. MHD mixed convection stagnation point flow of a hybrid nanofluid past a vertical flat plate with convective boundary condition. *Chin. J. Phys.* **2020**, *66*, 630–644. [CrossRef]
40. Ghalambaz, M.; Rosca, N.C.; Rosca, A.V.; Pop, I. Mixed convection and stability analysis of stagnation-point boundary layer flow and heat transfer of hybrid nanofluids over a vertical plate. *Int. J. Numer. Methods Heat Fluid Flow* **2020**, *30*, 3737–3754. [CrossRef]
41. Mahanthesh, B.; Shehzad, S.A.; Ambreen, T.; Khan, S.U. Significance of Joule heating and viscous heating on heat transport of MoS2–Ag hybrid nanofluid past an isothermal wedge. *J. Therm. Anal. Calorim.* **2021**, *143*, 1221–1229. [CrossRef]
42. Bilal, M.; Khan, I.; Gul, T.; Tassaddiq, A.; Alghamdi, W.; Mukhtar, S.; Kumam, P. Darcy-forchheimer hybrid nano fluid flow with mixed convection past an inclined cylinder. *Comput. Mater. Contin.* **2021**, *66*, 2025–2039. [CrossRef]
43. Lund, L.A.; Omar, Z.; Dero, S.; Chu, Y.; Khan, I.; Nisar, K.S. Temporal stability analysis of magnetized hybrid nanofluid propagating through an unsteady shrinking sheet: Partial slip conditions. *Comput. Mater. Contin.* **2021**, *66*, 1963–1975. [CrossRef]

44. Waini, I.; Ishak, A.; Pop, I. Hiemenz flow over a shrinking sheet in a hybrid nanofluid. *Results Phys.* **2020**, *19*, 103351. [CrossRef]
45. Waini, I.; Ishak, A.; Pop, I. Flow towards a stagnation region of a vertical plate in a hybrid nanofluid: Assisting and opposing flows. *Mathematics* **2021**, *9*, 448. [CrossRef]
46. Waini, I.; Ishak, A.; Pop, I. Hybrid nanofluid flow towards a stagnation point on an exponentially stretching/shrinking vertical sheet with buoyancy effects. *Int. J. Numer. Methods Heat Fluid Flow* **2021**, *31*, 216–235. [CrossRef]
47. Waini, I.; Ishak, A.; Pop, I. Hybrid nanofluid flow towards a stagnation point on a stretching/shrinking cylinder. *Sci. Rep.* **2020**, *10*, 9296. [CrossRef]
48. White, F.M. *Viscous Fluid Flow*, 3rd ed.; McGraw-Hill: New York, NY, USA, 2006.
49. Merkin, J.H. On dual solutions occurring in mixed convection in a porous medium. *J. Eng. Math.* **1986**, *20*, 171–179. [CrossRef]
50. Weidman, P.D.; Kubitschek, D.G.; Davis, A.M.J. The effect of transpiration on self-similar boundary layer flow over moving surfaces. *Int. J. Eng. Sci.* **2006**, *44*, 730–737. [CrossRef]
51. Harris, S.D.; Ingham, D.B.; Pop, I. Mixed convection boundary-layer flow near the stagnation point on a vertical surface in a porous medium: Brinkman model with slip. *Transp. Porous Media* **2009**, *77*, 267–285. [CrossRef]
52. Shampine, L.F.; Gladwell, I.; Thompson, S. *Solving ODEs with MATLAB*; Cambridge University Press: Cambridge, UK, 2003.